Supplemental Data

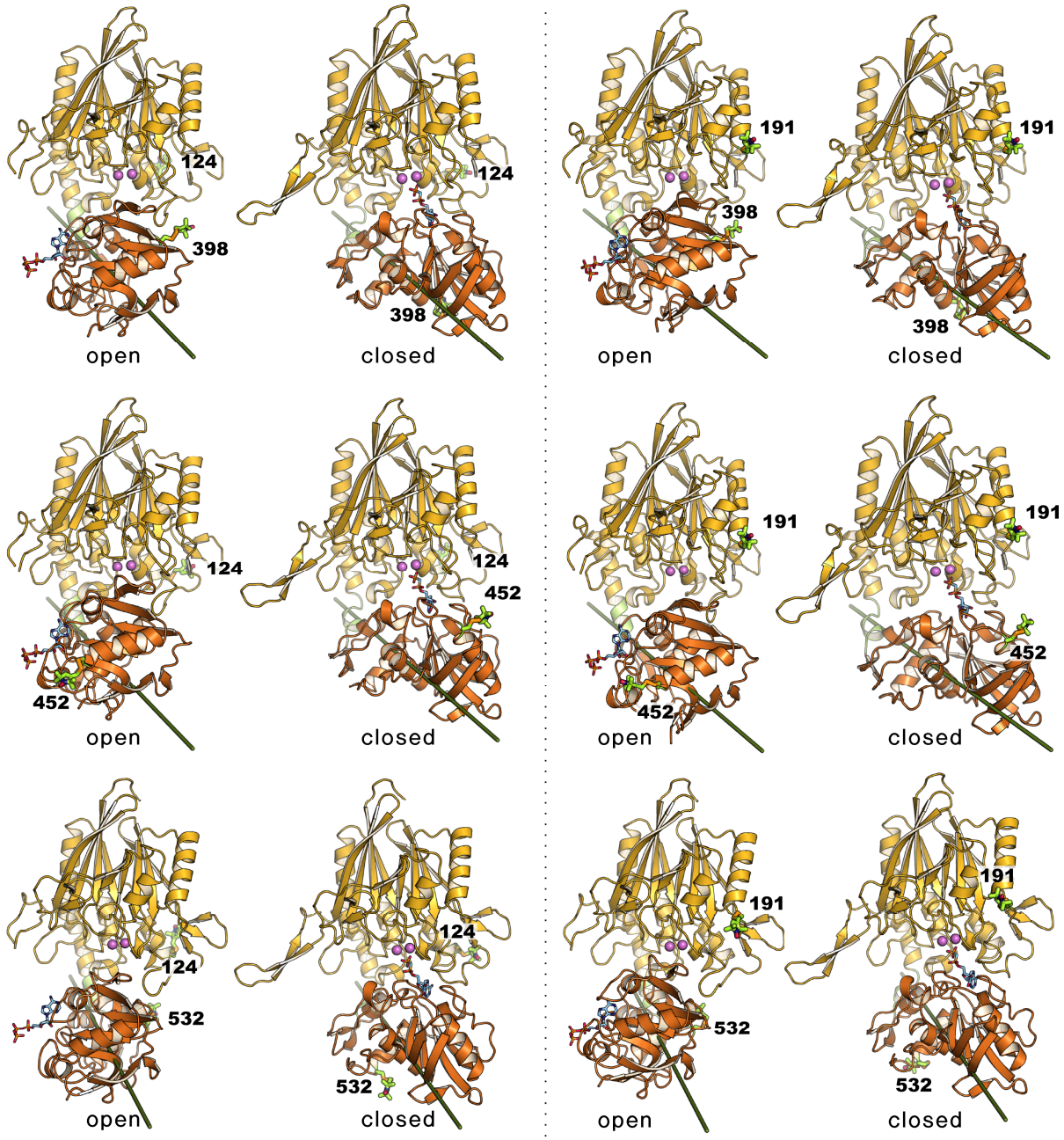

Figure S1 (related to Figure 1): 5NT variants in the open and closed conformations labeled with MTSSL. Six double cysteine mutants were prepared: T124C/G398C, T124C/Q452C, T124C/K532C, K191C/G398C, K191C/Q452C and K191C/K532C. The line through the center of the C-terminal domain marks the rotation axis between the two states.

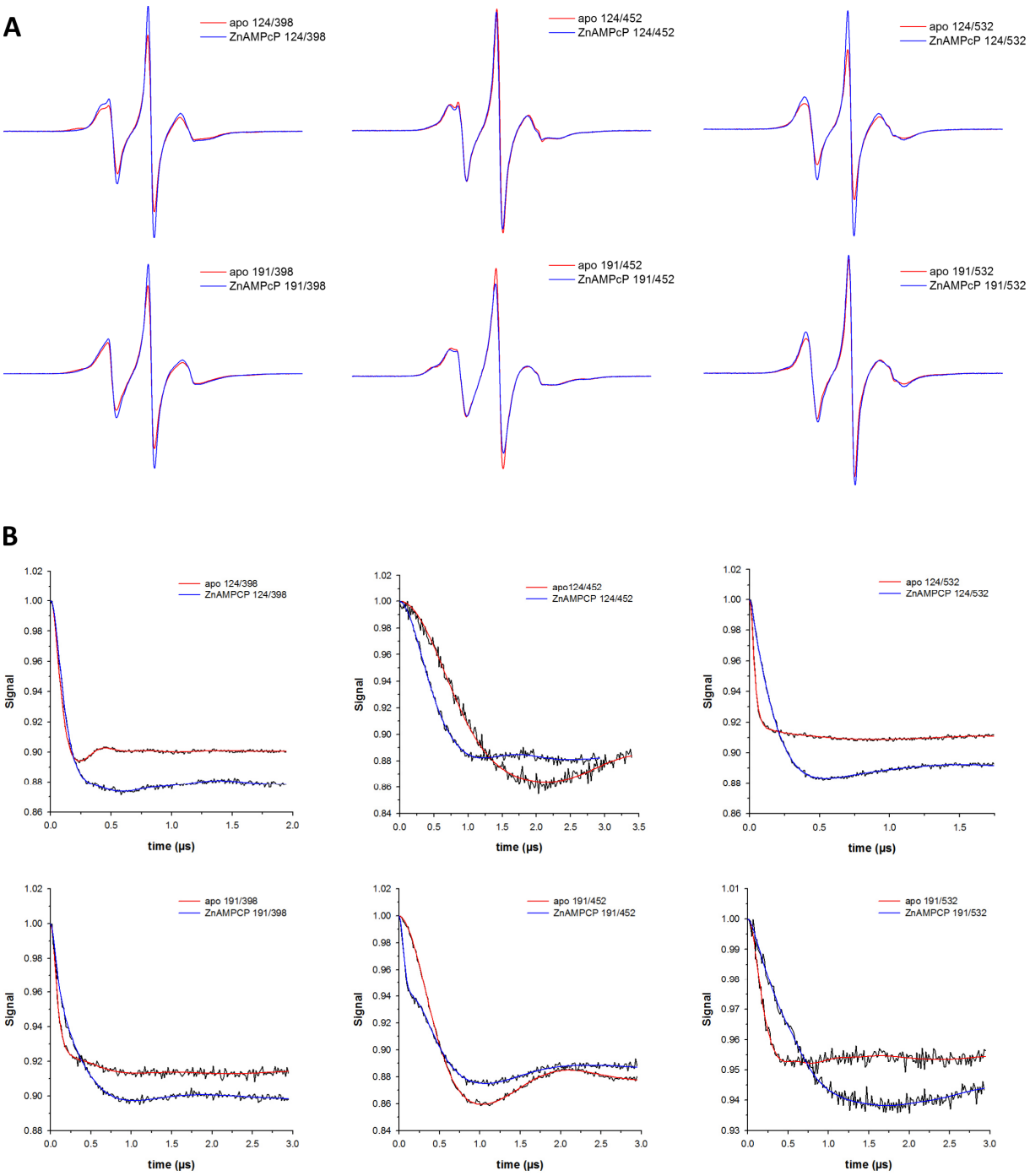

Figure S2 (related to Figure 2): CW-EPR spectra and DEER traces of MTSSL labeled 5NT variants in the apo (red) and ZnAMPCP-bound state (blue). A) CW-Spectra were collected on a Bruker EMX spectrometer using 10 mW microwave power level and a modulation amplitude of 1.6 G. **B)** DEER spectroscopy was performed on a Bruker 580 pulsed EPR spectrometer operating at Q-band frequency (33.9 GHz) with a standard four-pulse protocol at 83 K. Numbers indicate spin-labeled 5NT mutants T124C/G398C, T124C/Q452C, T124C/K532C, K191C/G398C, K191C/Q452C and K191C/K532C.

MTSSL labeling at residues 124/398

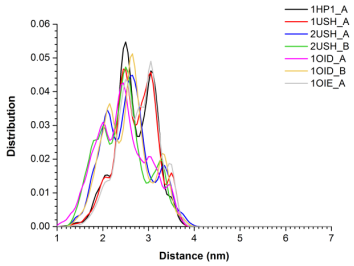

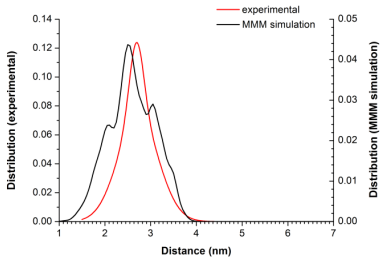

MTSSL labeling at residues 124/452

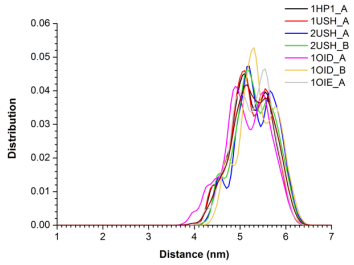

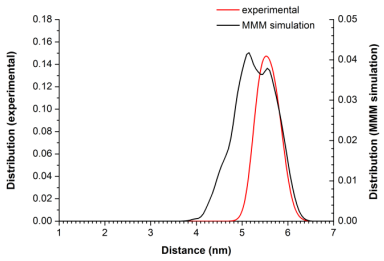

MTSSL labeling at residues 124/532

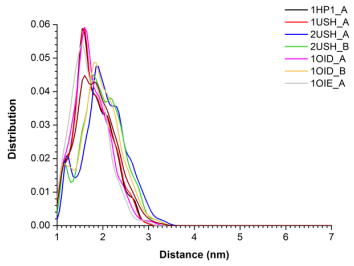

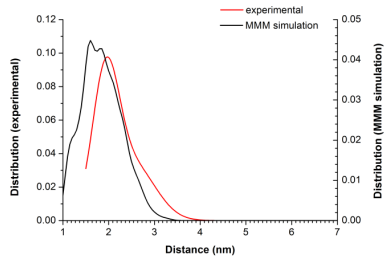

MTSSL labeling at residues 191/398

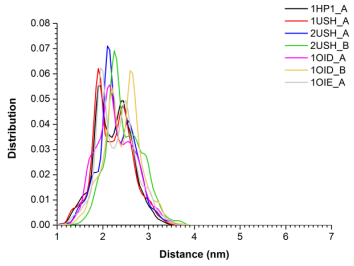

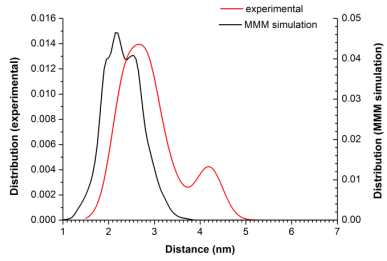

MTSSL labeling at residues 191/452

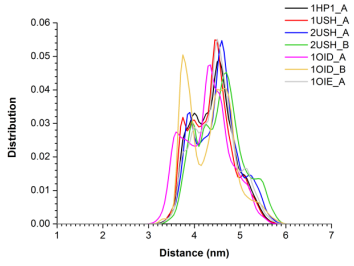

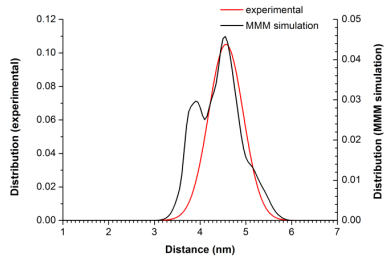

MTSSL labeling at residues 191/532

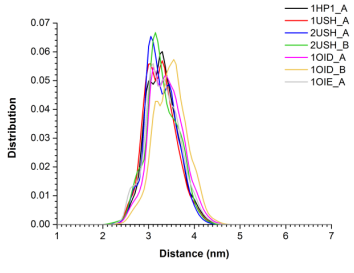

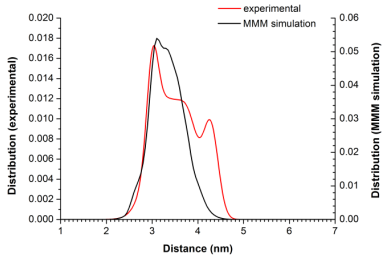

Figure S3 (related to Figure 2): Simulation of DEER distance distributions for 5NT variants with rotamer library from MMM. The program MMM was used to simulate the distance distributions of the six 5NT double mutants for seven open conformations (left). The "average" distance distribution of the seven open conformations is compared to the experimentally obtained DEER data (right).

Ensemble fit with crystal structures

apo data

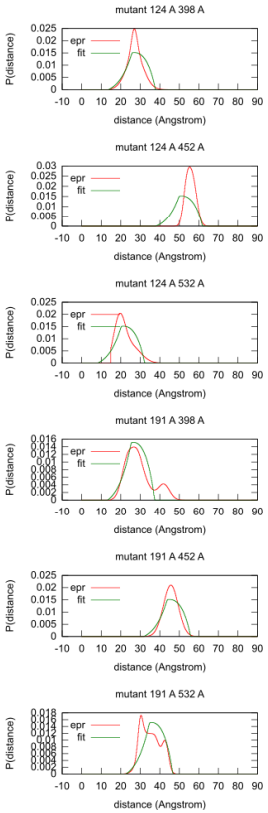

bcl::storage::Table<double>	weight	value	weighted_val
mutant_124_A_398_A	1.0000	0.0338	0.0338
mutant_124_A_452_A	1.0000	0.1062	0.1062
mutant_124_A_532_A	1.0000	0.0315	0.0315
mutant_191_A_398_A	1.0000	0.0453	0.0453
mutant_191_A_452_A	1.0000	0.0265	0.0265
mutant_191_A_532_A	1.0000	0.0477	0.0477
ensemble_size	40.0000	0.0006	0.0250
sum	46.0000	0.2916	0.3160

ensemble:
1× 1OID_open_B

ZnAMPCP data

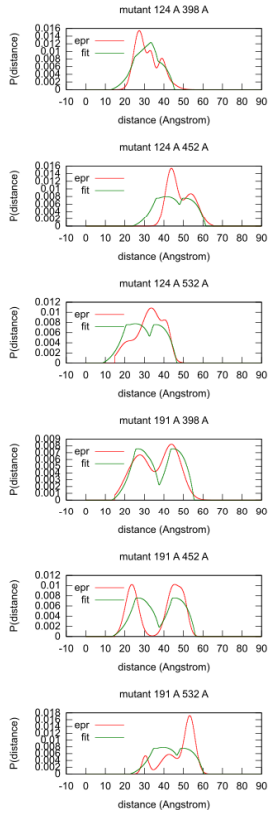

bcl::storage::Table<double>	weight	value	weighted_val
mutant_124_A_398_A	1.0000	0.0195	0.0195
mutant_124_A_452_A	1.0000	0.0772	0.0772
mutant_124_A_532_A	1.0000	0.0594	0.0594
mutant_191_A_398_A	1.0000	0.0192	0.0192
mutant_191_A_452_A	1.0000	0.0476	0.0476
mutant_191_A_532_A	1.0000	0.0881	0.0881
ensemble_size	40.0000	0.0013	0.0013
sum	46.0000	0.3122	0.3610

ensemble:
1× 2USH_open_B
1× 1HPU_closed_A

Ensemble fit with MD models

apo data

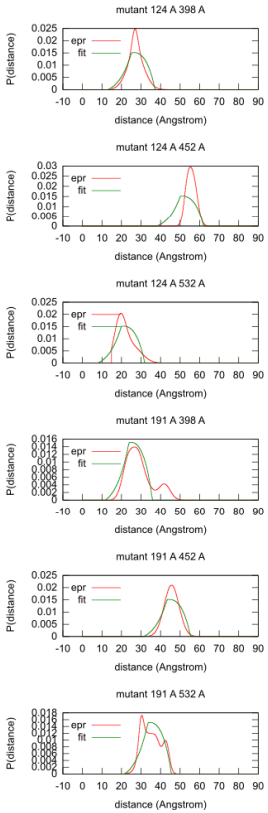

bcl::storage::Table<double>	weight	value	weighted_val
mutant_124_A_398_A	1.0000	0.0250	0.0250
mutant_124_A_452_A	1.0000	0.1014	0.1014
mutant_124_A_532_A	1.0000	0.0268	0.0268
mutant_191_A_398_A	1.0000	0.0678	0.0678
mutant_191_A_452_A	1.0000	0.0229	0.0229
mutant_191_A_532_A	1.0000	0.0250	0.0250
ensemble_size	40.0000	0.0007	0.0267
sum	46.0000	0.2696	0.2956

ensemble: **χ1 (χ2)**
1×MD-27 93° (3.1°)

ZnAMPCP data

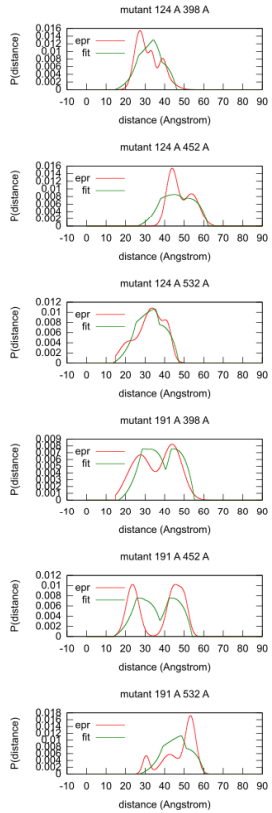

bcl::storage::Table<double>	weight	value	weighted_val
mutant_124_A_398_A	1.0000	0.0342	0.0342
mutant_124_A_452_A	1.0000	0.0485	0.0485
mutant_124_A_532_A	1.0000	0.0145	0.0145
mutant_191_A_398_A	1.0000	0.0423	0.0423
mutant_191_A_452_A	1.0000	0.0627	0.0627
mutant_191_A_532_A	1.0000	0.0637	0.0637
ensemble_size	40.0000	0.0013	0.0533
sum	46.0000	0.2672	0.3192

ensemble: **χ1 (χ2)**
1× MD-54 78° (4.1°)
1× MD-280 7° (2.6°)

Ensemble fit with docked models

apo data

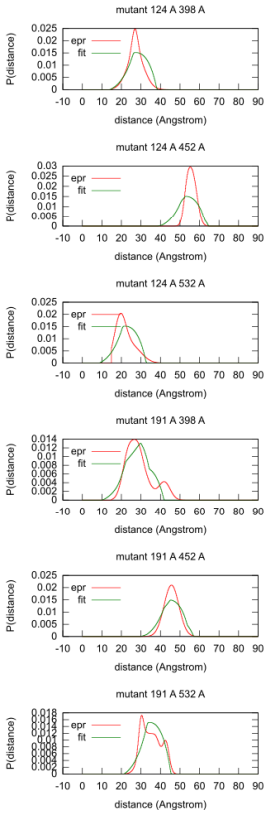

bcl::storage::Table<double>	weight	value	weighted_val
mutant_124_A_398_A	1.0000	0.0429	0.0429
mutant_124_A_452_A	1.0000	0.0679	0.0679
mutant_124_A_532_A	1.0000	0.0402	0.0402
mutant_191_A_398_A	1.0000	0.0302	0.0302
mutant_191_A_452_A	1.0000	0.0268	0.0268
mutant_191_A_532_A	1.0000	0.0228	0.0228
ensemble_size	40.0000	0.0007	0.0267
sum	46.0000	0.2315	0.2575

ensemble: **χ1 (χ2)**
1× c19 60° (28.9°)
1× o437 110° (21.2°)

ZnAMPCP data

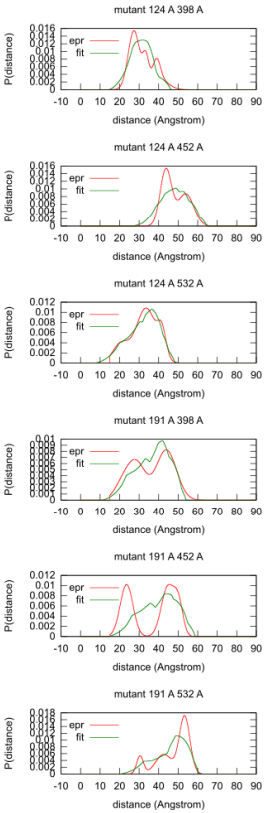

bcl::storage::Table<double>	weight	value	weighted_val
mutant_124_A_398_A	1.0000	0.0220	0.0220
mutant_124_A_452_A	1.0000	0.0249	0.0249
mutant_124_A_532_A	1.0000	0.0090	0.0090
mutant_191_A_398_A	1.0000	0.0320	0.0320
mutant_191_A_452_A	1.0000	0.0830	0.0830
mutant_191_A_532_A	1.0000	0.0369	0.0369
ensemble_size	40.0000	0.0013	0.0533
sum	46.0000	0.2093	0.2613

ensemble: **χ1 (χ2)**
1× c170 14° (8.0°)
1× o375 38° (16.5°)
1× o331 67° (6.4°)
1× o84 122° (21.6°)

Figure S4 (related to Figure 3): Ensemble fit of 5NT EPR distance distributions with crystal structures, MD and docked models. The experimental data (red) and the fit with the given ensemble (green) are plotted for the apo and the ZnAMPCP data. Histograms are shown for ensemble fitting with a weight for the ensemble size (w_E) of 40. Statistics reflect the contribution of each mutant to the total score T ("sum") in ensemble fitting. The composition of each ensemble is given.

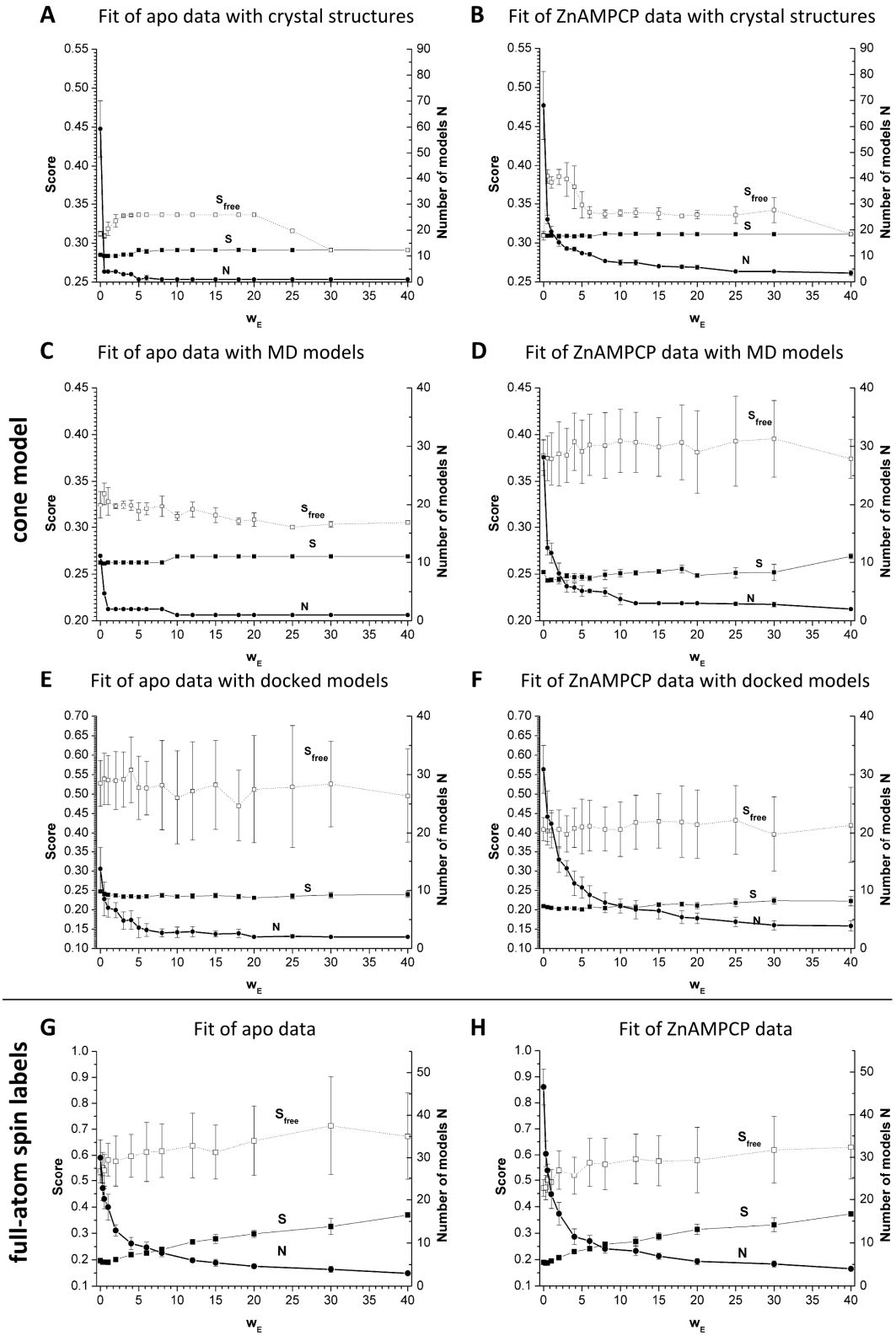

Figure S5 (related to Figure 5): Ensemble fitting based on the knowledge-based potential of the cone model (A-F) or with full-atom models of MTSSL attached to 5NT crystal structures (G-H). Given is the dependency of the Score (S), the free Score (S_{free}) and the number of models in the ensemble (N) on the weighting term for the ensemble size score (w_E). Distance distributions of 5NT in the apo and in the inhibitor-bound ZnAMPCP state were ensemble fitted with crystal structures, MD models or docked models for different w_E. Indicated values are the average of the best 10% of the fits with their standard deviations. For each weighting term the resulting *S* (-■-), S_{free} (··□··) and N (-●-) is given.

Table S1 (Related to Figure 4): Classification of 300 models derived from targeted MD simulation of the 5NT domain motion. The classification is based on the χ_1 angle as defined by the linear path analysis of the closed-to-open-rotation of structures 1HPU_C to 1HP1_A.

Classification of MD-models	Range of MD-models	Rotational range χ_1
open	MD-1 to MD-45, MD-47	$105.5 \leq \chi_1 \leq 80.0°$
int. 1	MD46, MD-48 to MD-66	$80.0° < \chi_1 \leq 65.0°$
int. 2	MD-67 to MD-90	$65.0° < \chi_1 \leq 50.0°$
int. 3	MD-91 to MD-141	$50.0° < \chi_1 \leq 35.0°$
int. 4	MD-142 to MD-167, MD-169, MD-172, MD-174, MD-175	$35.0° < \chi_1 \leq 20.0°$
closed	MD-168, MD-170, MD-171, MD-173, MD-176 to MD-300	$20.0° < \chi_1 \leq 0.0°$

Table S2: Classification of 1000 models derived from docking of the N- and C-terminal domains of 5NT (Related to Figure 4). The classification is based on the χ_1 angle as defined by the linear path analysis of the closed-to-open-rotation of structures 1HPU_C to 1HP1_A.

	Classification of docked models	Rotational range χ_1
1	more-open	$105° < \chi_1$
2	Open	$105° \leq \chi_1 \leq 80°$
3	int. 1	$80° < \chi_1 \leq 65°$
4	int. 2	$65° < \chi_1 \leq 50°$
5	int. 3	$50° < \chi_1 \leq 35°$
6	int. 4	$35° < \chi_1 \leq 20°$
7	Closed	$20° < \chi_1 \leq -5°$
8	more-closed	$-5° > \chi_1$

Table S3 (Related to Table 1): Detailed summary of the results of the best LOO-fit for crystal structures, MD models and models from docking of the domains at a weighting term $w_E = 40$.

crystal struct.	apo		ZnAMPCP	
	ensemble	Score	ensemble	Score
all	1OID_B	0.291	1HPU_A 2USH_B	0.311
124/398	1OID_B	0.0338	1HPU_A 2USH_B	0.0195
124/452	1OID_B	0.1062	1HPU_A 2USH_B	0.0772
124/532	1OID_B	0.0315	1HPU_A 2USH_B	0.0594
191/398	1OID_B	0.0453	1HPU_A 2USH_B	0.0192
191/452	1OID_B	0.0265	1HPU_A 2USH_B	0.0476
191/532	1OID_B	0.0477	1HPU_A 2USH_B	0.0881

MD models		apo			ZnAMPCP			
	ensemble	χ_1	χ_2	Score	ensemble	χ_1	χ_2	Score
all	MD-27	93°	3.1°	0.2689	MD-280 MD-54	7° 78°	2.6° 4.1°	0.2759
124/398	MD-27	93°	3.1°	0.0250	MD-180 MD-54	15° 78°	6.5° 4.1°	0.0435
124/452	MD-28	92°	4.0°	0.1076	MD-277 MD-54	7° 78°	2.2° 4.1°	0.0591
124/532	MD-27	93°	3.1°	0.0268	MD-280 MD-35	7° 90°	2.6° 4.3°	0.0570
191/398	MD-27	93°	3.1°	0.0678	MD-280 MD-54	7° 78°	2.6° 4.1°	0.0423
191/452	MD-27	93°	3.1°	0.0229	MD-173 MD-54	18° 78°	9.0° 4.1°	0.0873
191/532	MD-37	89°	4.1°	0.0557	MD-295 MD-35	7° 90°	5.0° 4.3°	0.0890

docking models		apo			ZnAMPCP			
	ensemble	χ_1	χ_2	Score	ensemble	χ_1	χ_2	Score
all	o437 c19	110° 60°	21.2° 28.9°	0.2308	o84 o331 o375 c170	122° 67° 38° 14°	21.6° 6.4° 16.5° 8.0°	0.208
124/398	o437 c19	110° 60°	21.2° 28.9°	0.0429	o437 o331 c242 c65	110° 67° 20° 19°	21.2° 6.4° 13.4° 11.1°	0.0232
124/452	o429 c19	147° 60°	39.1° 28.9°	0.1657	o473 o465 c340 c45	144° 85° 20° 11°	34.5° 7.6° 10.7° 17.3°	0.1110
124/532	o437 c19	110° 60°	21.2° 28.9°	0.0402	o104 o465 c242 c65	126° 85° 20° 19°	42.6° 7.6° 13.4° 11.1°	0.0131
191/398	o437	110°	21.2°	0.0995	c82 o216 c355 c182	76° 54° 46° -3°	16.2° 33.3° 23.4° 8.7°	0.0803
191/452	o264 c19	122° 60°	23.8° 28.9°	0.0478	o84 o331 c435 o161	122° 67° 46° 27°	21.6° 6.4° 4.2° 14.4°	0.1365
191/532	o437 c19	110° 60°	21.2° 28.9°	0.0228	o342 c341 c92	97° 40° -7°	12.1° 14.8° 6.2°	0.1005

Supplemental Experimental Procedures

Preparation of 5NT mutants used for EPR spin labeling

To prepare the six 5NT double cysteine mutants T124C/G398C, T124C/Q452C, T124C/K532C, K191C/G398C, K191C/Q452C and K191C/K532C the gene coding for 5NT cloned in the pET28a(+) vector (Krug et al., 2013) was modified by site-directed mutagenesis via the QuikChange Mutagenesis protocol (Stratagene). The following sense mutagenesis primers were used: 5'-GAT AAT CCG CTC TGC GTA TTA CGC CAG CAG G-3' for T124C, 5'-GAT ATC GAA TTT CGT TGC CCC GCC GAT GAA GCG AAG C-3' for K191C, 5'-C CAA ATG GAT CGC ACT TGC GCC GAC TTT GCG GTG-3' for G398C, 5'-CTG ACC GCC GTC GCG TGC ATG AAG CCA GAT TCA GG-3' for Q452C and 5'-G CTG AAA GCG TAT ATC CAG TGC AGC TCG CCG CTG GAT GTG-3' for K532C (point mutations are underlined). The modified 5NT genes containing the natural disulfide C258/C275 plus two additional cysteines were expressed in *E. coli* BL21(DE3) or Rosetta pLysS cells. The 25 amino acid long signal sequence was cleaved off after secretion into the periplasm resulting in a protein of amino acids Y26 to Q550, with the introduced mutations and followed by the artificial C-terminal LEHHHHHH-sequence. Purification was carried out as described before by affinity, ion exchange and size exclusion chromatography (Schultz-Heienbrok et al., 2004; Krug et al., 2013). 1 mM DTT was added to all buffers during purification of the protein to prevent formation of disulfides by the artificial cysteines.

The specific enzymatic activity (U/mg) was determined by the release of phosphate after enzymatic turnover of AMP using a modified malachite green assay as detailed before (Krug et al., 2013).

Coupling of MTSSL to free cysteine residues

1-oxyl-2,2,5,5-tetramethylpyrroline-3-methyl methanethiosulfonate (MTSSL, purchased from Toronto Research Canada via LGC Standards GmbH, Wesel/Germany) was dissolved in anhydrous DMF and stored as 100 mM stock solution at -80°C. For labeling the protein buffer was changed to 9 mM Tris, 6 mM MES, 50 mM NaCl, 0.1 mM EDTA and 3 mM NaN_3 (pH 7.2) on a 5 mL HiTrap Desalting column (GE Healthcare) to remove DTT. Then a tenfold excess of MTSSL over protein was added, followed by two hours of incubation at room temperature and another addition of MTSSL

(again a tenfold excess). The mixture was incubated at 4°C over night. Finally, unreacted spin label was removed by a 53 mL HiTrap Desalting column (GE Healthcare) with 20 mM Tris, 50 mM KCl and 0.5 mM EDTA (pH 8.5).

Data acquisition of EPR distance distributions

After labeling protein samples were frozen in liquid nitrogen and transferred to Nashville on dry ice within 3 days. Glycerol (30% w/w) was added as cryoprotectant. To provide samples in the inhibitor-bound state 5 mM AMPCP (Sigma Aldrich/Germany) and 0.5 mM $ZnCl_2$ were added before freezing. Due to a K_i of 0.25 µM the concentration of AMPCP corresponds to a saturating amount of inhibitor. For CW-EPR, spin-labeled 5NT samples were loaded in capillaries and spectra were collected on a Bruker EMX spectrometer using a 10 mW microwave power level and a modulation amplitude of 1.6 G. DEER spectroscopy was performed on a Bruker 580 pulsed EPR spectrometer operating at Q-band frequency (33.9 GHz) with a standard four-pulse protocol at 83 K (Jeschke, 2002). Analysis of the DEER data to determine the distance distributions, P(r), was carried out in DeerAnalysis 2011 (Jeschke et al., 2006). The data were fitted with Tikhonov regularization and L-curve determination of the optimal regularization parameter (Chiang et al., 2005).

Supplemental References

Chiang, Y.W., Borbat, P.P., and Freed, J.H. (2005). Maximum entropy: a complement to Tikhonov regularization for determination of pair distance distributions by pulsed ESR. J.Magn Reson. *177*, 184-196.

Jeschke, G. (2002). Distance measurements in the nanometer range by pulse EPR. Chemphyschem. *3*, 927-932.

Jeschke, G., Chechik, V., Ionita, P., Godt, A., Zimmermann, H., Banham, J., Timmel, C.R., Hilger, D., and Jung, H. (2006). DeerAnalysis2006- a comprehensive software package for analyzing pulsed ELDOR data. Applied Magnetic Resonance *30*, 473-498.

Krug, U., Patzschke, R., Zebisch, M., Balbach, J., and Sträter, N. (2013). Contribution of the two domains of E. coli 5'-nucleotidase to substrate specificity and catalysis. FEBS Lett. *587*, 460-466.

Schultz-Heienbrok, R., Maier, T., and Sträter, N. (2004). Trapping a 96 degrees domain rotation in two distinct conformations by engineered disulfide bridges. Protein Sci. *13*, 1811-1822.